ACS APPLIED MATERIALS & INTERFACES

Research Article

www.acsami.org

Self-Assembled Monolayer-Based Selective Modification on Polysilicon Nanobelt Devices

Hao Heng Liu, Tzung Han Lin, and Jeng-Tzong Sheu*

Institute of Nanotechnology/Department of Materials Science and Engineering, National Chiao Tung University, 1001 Ta Hsueh Road, Hsinchu, Taiwan 30050

Supporting Information

ABSTRACT: In this study, a self-assembled monolayer (SAM) of methoxy-poly (ethylene-glycol)-silane (mPEG-sil) was used to modify the silicon dioxide surface of polysilicon nanodevices (PNDs) to act as a passivation layer that inhibits nonspecific binding of proteins and reduces localized Joule heating power. Selective modifications of 3-aminopropyltrimethoxysilane (APTMS), NHS-biotin and dye-labeled Streptavidin on the removal regions were characterized. These PNDs, which consist of a two-level doping profile, were designed to confine heat in the low-level doping region during localized Joule heating. Localized Joule heating with pulse bias was examined in both vacuum and ambient, which indicated the removal region was longer in vacuum for the same pulse bias. Moreover, a comparison of selectively and nonselectively modified PNDs observed in time-lapsed fluorescence detection of dye-labeled Streptavidin showed a higher increasing rate in fluorescence intensity (~2× enhancement) in the selectively modified PNDs. Finally, a COMSOL simulation was employed to evaluate the temperature distribution in the PNDs, with results showing that heat confinement was observed in the low-level doping region and a temperature very close to 673 K was achieved while applying a pulse voltage (40 V, 5 μs) to remove mPEG-sil.

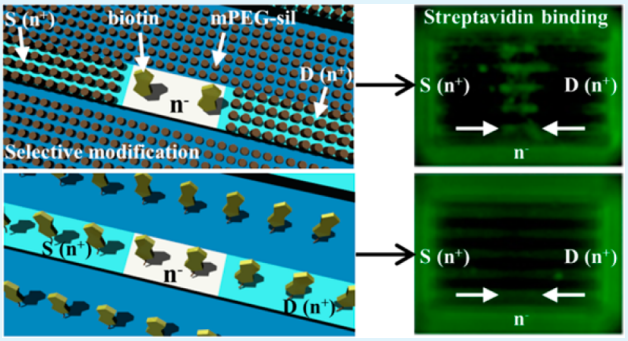

KEYWORDS: *polysilicon nanobelts, localized Joule heating, self-assembled monolayer, selective modification*

1. INTRODUCTION

There is growing interest in applications of silicon nanodevices in the biosensing. Silicon nanodevices own high sensitivity to changes of surface potential that are caused by the charged targets binding on the modified surface. Research has reported using silicon nanodevices as sensing platforms to detect viruses, proteins, DNAs, and noncharged molecules.[1−8] Although the limit of detection (LOD) has been pushed to the subpicomolar level, sensing time still remains a limitation. Both simulation and experimental results have shown that blocking the nonsensing regions on the device can reduce the sensing time and improve detection sensitivity, especially at very low target concentrations.[9−12] Several studies have demonstrated selective modifications. Photolithography[13] provides high accuracy in alignment, but the machine cost is high for nanoscale process. Micro contact printing[14] (μCP) provides simple process, but the accurate alignment in nanoscale is still hard to control. Two PDMS-based site-selective deposition methods provide another route for selective modifications. One used a polydimethylsiloxane (PDMS) micro mold combined with gas-phase deposition for nanoscale modification on specific site of chip[15] and the other used PDMS mold as a soft contact mask in plasma etching to achieve selective patterning.[16] However, the alignment accuracy of these techniques still in the realm of μCP. Dip-pen nanolithography,[17] which based on AFM system, provides addressing ability in nanometer region, but the addressing speed is very slow. Laser-induced patterning[18] provides direct-writing ability to define submicrometer pattern for selective modification but it takes tens of seconds in process. None of those techniques have been attempted for high selectivity modification of bio- or chemical molecules on high sensitive regions of PNDs. Recently, two selective surface modification methods on nanowires or nanobelts, one bottom-up and one top-down method, have been demonstrated. Li's work[12] presented a bottom-up modification of chemical linkers on silicon nanowire before forming the contacts of nanowire field-effect transistor (FET). Despite the high selectivity in surface modification, the electrical contact properties of nanowire FET could be undermined because of the existence of chemical linker between metal pads and silicon channel. In contrast, Park's work,[19] a top-down method, used the localized Joule heating to ablate the PTFE film on the silicon nanowire devices for the further surface modifications. However, the PTFE is hard to ablate via heat because of its high boiling point and is hydrophobic, which could undermine the contact between the

Received: July 1, 2013
Accepted: September 11, 2013
Published: September 11, 2013

analyte and the PND. Researchers used the PMMA[20] as a passivation material and demonstrate same function as well. Nonetheless, PMMA usually causes nonspecific binding during real-time detection, and it still needs an additional process to passivate the nonreacted regions and may cause contamination on the modified molecules into ablated regions during the removal of PMMA. The mPEG-sil layer has been employed and recognized for its ability to reduce the nonspecific binding on the oxide surface[21,22] because of its high compact structure during formation of the SAM. In this research, mPEG-sil SAM, instead of polymer film, was used as a protection layer to resist nonspecific binding of protein and to reduce localized Joule heating power. Localized Joule heating was performed in vacuum to maximize the removal region on the PND. In addition, mPEG-sil is stable in vacuum after covalent bonding to the sample surface, whereas the polymer film usually generates bubbles in vacuum and creates nonuniform thickness in polymer film. Finally, conjugation of dye-labeled Streptavidin with modified biotin is used to demonstrate good resistivity of mPEG-sil in nonspecific binding, good selectivity of modification of biotin on the removal region, and an improvement of sensing time as indicated by time-lapsed fluorescence observation.

2. EXPERIMENTAL SECTION

2.1. Device Fabrication. The PNDs were prepared by fully CMOS compatible processes. A p-type silicon wafer was grown with 1000 Å-thick thermal oxide after a standard RCA clean process. A 600 Å-thick polysilicon film was deposited by LPCVD and patterned by conventional optical lithography, and then n^- regions were implanted with 4×10^{14} cm^{-2} of phosphorus at 20 keV. The n^+ regions were implanted with 3×10^{15} cm^{-2} of arsenic at 30 keV. Subsequently, an oxide/nitride stack with thicknesses of 4.5/5.5 nm, respectively, was deposited by LPCVD. After interlevel dielectric (ILD) deposition, dopants were activated at 930 °C for 30 min in a furnace. After forming the contact via, a metallization process was followed by forming gas annealing at 400 °C to obtain an Ohmic contact. Finally, the sensing window was opened by etching of top Si_3N_4 passivation layer and ILD, sequentially.

2.2. Surface Modification. *2.2.1. Immobilization of mPEG-sil and APTMS.* PNDs were cleaned by UV/ozone prior to mPEG-sil (Gelest) deposition. The mPEG-sil (M_w = 460−590 Da) was prepared to a concentration of 6 mM in anhydrous toluene with 1% tetraethyl ammonium (TEA) acting as a catalyst and then reacted for 24 h on a hot plate at 60 °C. After termination of this reaction, the PNDs were subsequently cleaned with anhydrous toluene and alcohol for 5 min to remove unreacted molecules. Finally, devices were rinsed with DI water and blown dry in a nitrogen stream. 3-aminopropyltrimethoxysilane (APTMS) (Sigma) with a concentration of 2 mM in DI water was deposited for 10 min and washed three times with DI water in an ultrasonicator, and then blown dry by a nitrogen stream.

2.2.2. Biotin Grafting and Streptavidin Binding. In the case of Streptavidin binding, 1 mg of NHS-biotin (Thermal Scientific) was first dissolved in 150 μL of DMSO and then diluted with 850 μL 1X PBS to a total volume of 1 mL. The NHS amide bonds were allowed to react with the amino groups of APTMS for 2 h. PNDs were then washed by DI water and blown dry with a nitrogen stream. Finally, 10 μg/mL of Alexa Fluor 488 Streptavidin (Invitrogen) with 0.1% Tween20 in 0.01X PBS (PBST) was dropped onto the PNDs and reacted with NHS-biotin for 1 h. For the case of time-lapsed observation, the Streptavidin was delivered by peristaltic pump through a 1.6 μL microfluidic channel with a flow rate of 100 μL/min for 30 s and washed three times with 1X PBST by ultrasonication.

2.3. Joule Heating and Characterization. The resistance of PND was measured by Agilent 4156C prior to localized Joule heating via a probe station in both vacuum and ambient. Localized Joule heating was then carried out by Agilent 41501B Pulse Generator in both vacuum (2×10^{-3} Torr) and ambient. AFM images including topography and phase signal were captured by a JEOL SPM-5200. The AFM scanning utilized an aluminum-coated silicon tip (Budget Sensors) with a force constant of 40 N/m and the resonant frequency of 300 kHz. The scanning speed is 4 μm/s. The fluorescence images were characterized by a confocal microscope and a Carl Zeiss upright microscope (Axio scope A1). Water contact angle measurements were performed by adding a 1 μL of DI water droplet on chip and then use the camera taking images. Furthermore, these images were analyzed by a FTA32 software.

2.4. COMSOL Simulation. Simulations based on the finite element method (FEM) were performed using COMSOL Multiphysics software. The simulation structure was simplified to reduce the calculation time because of the large amount of mesh numbers; The PNDs were laid on a 150-nm buried oxide. The pads of PNDs were ignored in calculations, with the nitride/oxide stack passivation layer on the nanobelts stacked to cover only the n^- regions and extending 1 μm from both ends of the n^- regions. The thickness of the nitride and oxide in the layer was 5.5 and 4.5 nm, respectively. The resistivity of PND in n^- and n^+ regions was 3.125×10^{-1} and 8.125×10^{-3} Ω cm, respectively, and temperature coefficient of resistance was -1.2×10^{-3} k^{-1} as obtained by an Agilent 4156C semiconductor parameter analyzer. The contacts were located on the ends of the five polysilicon nanobelts, with the ends on one side set to ground while those on the other were applied 33.6 and 41.9 V, corresponding to 40 and 50 V pulse voltage, respectively, according to the voltage division principle. The initial temperature for all boundaries was set to 298 K.

3. RESULTS AND DISCUSSION

A process flow of simple one-step selective modification was depicted in Figure 1. For the selectively modified case, the surface of the PND chip was first modified with mPEG-sil, which was subsequently removed selectively by localized Joule

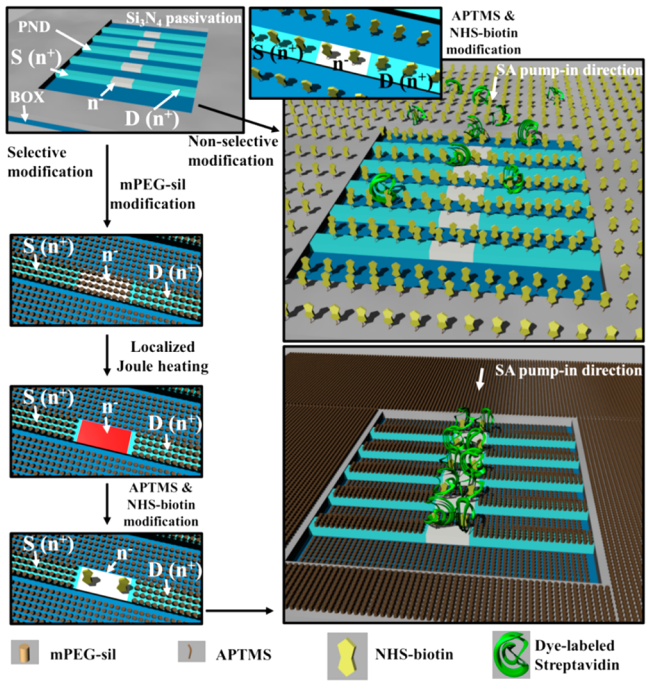

Figure 1. Schematic process flow of selective modification, for both selective and nonselective modification. PNDs were modified with mPEG-sil for the selectively modified case then localized Joule heating was performed. Subsequently, APTMS and NHS-biotin were deposited on both selectively and nonselectively modified devices. Finally, dye-labeled Streptavidin was delivered and bound to the two kinds of chips.

heating in both vacuum and ambient. The linkers, APTMS and NHS-biotin, were sequentially used to modify in the removal regions.

Conversely, the control sample (chip without localized Joule heating) was modified with linkers on the whole device. Finally, Alexa Fluor 488-conjugated Streptavidin was bound on the biotin and used to verify the removal of mPEG-sil and to evaluate the sensing time by time-lapsed observation of fluorescence on PNDs.

The structure of PNDs is shown in Figure 2. Each device, consisting of 5 polysilicon nanobelts in parallel, was connected to two silicon pads (Figure 2a).

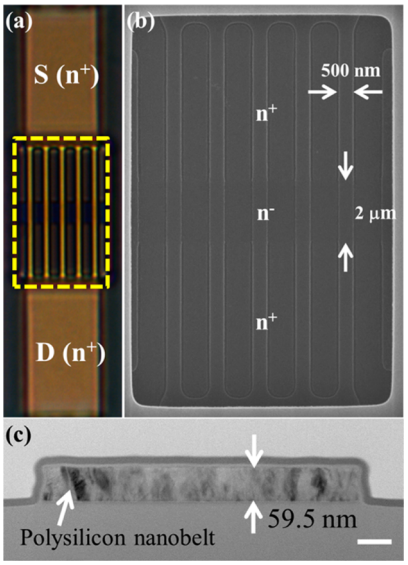

Figure 2. (a) Optical image of PND, S and D representing the source and drain. (b) SEM image of the area marked in yellow in a, with n^+ and n^- representing the doping level at the corresponding regions. Nanobelt dimensions are highlighted in the figure. (c) Cross-sectional TEM image of a nanobelt. Nanobelt thickness is labeled on the figure. Scale bar: 50 nm.

PND channels possess three doping regions of a 2 μm long n^- region in the middle of the nanobelts, and two 5.5 μm long n^+ distal regions for each nanobelt. The dimensions of the nanobelts were marked in Figure 2b,c. The resistance of the PND in n^- and n^+ regions is 37.96 and 4.24 kΩ, respectively, which implies the power applied on n^- regions is ca. 9-fold larger than on the n^+ regions; The sheet resistance of n^-, n^+, and contact via was 13.32, 1, and 1.84 $\Omega/\square$, respectively; the calculated resistances according to the dimensions of each part of the PND were in good agreement with the measurement results. This design causes most of the Joule heating power to be dissipated mainly in the n^- regions and constrains hot zones within the n^- regions. Similar results have been demonstrated where material on hot zones was ablated by heat, while not ablated on n^+ regions.[20] Park et al. have demonstrated nanoscale Joule heating using uniform doped nanodevice.[19] The doping level of device channel was reported to be 1×10^{18} cm^{-3}. However, the high resistance takes longer heating time and higher power to remove the passivation materials. Moreover, the low doping concentration usually causes the contact problem due to the formation of the Schottky contact between metal and silicon channel. On the other hand, high channel doping level shortens the device debye screen length and thus reduce the device sensitivity to the change of surface potential.

The mPEG-sil is used as a passivation layer to resist the nonspecific protein binding. The surface modification of mPEG-sil SAM was characterized by AFM and contact angle measurement. Figure 3 presents surface roughness and contact

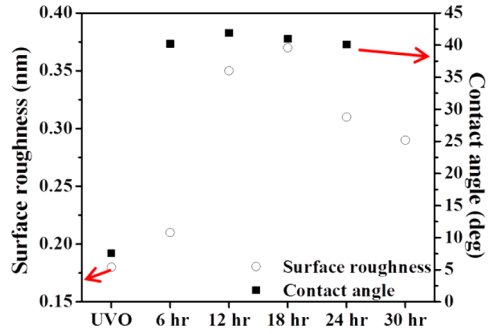

Figure 3. Plot of surface roughness and contact angle variations vs process time. The surface roughness marked with open circle (○) corresponds to the value on the left *y*-axis. The contact angle marked with solid black block (■) corresponds to the value on the right *y*-axis. "UVO" and the time shown on *x*-axis represent the process and the modification time of mPEG-sil, respectively.

angle after various periods of surface modification of mPEG-sil. The chip was first treated with UV/ozone for 30 min, so the contact angle (solid black block) was very close to 0°. It increased drastically from 7.5 to 40° during the first 6-h modification time, and changed only slightly until 24 h. The constant contact angle is coincident with the results reported by several research teams.[23,24] AFM offers more detailed information on surface modification in nanoscale. The surface roughness increases from 0.18 to 0.21 nm during the first 6 h and then increases dramatically to 0.35 nm in the next 6 h. It reaches a maximum (0.37 nm) at the eighteenth hour, and then drops back to 0.31 nm at the twenty fourth hour and remains at the same level after the twenty fourth hour. The increment of roughness results from the initiation of binding mPEG-sil onto the chip surface its gradual increase in density. The decrement after the eighteenth hour implies formation of a uniform thin layer, and that the vacancies of the mPEG-sil film have become filled. Therefore, the optimized deposition time of mPEG-sil was set to 24 h.

Figure 4 shows the relationship between the localized Joule heating and applied power in both vacuum and ambient. The removal length of mPEG-sil along the long axis of the nanobelt exhibited a linear relationship to the square of bias voltage. The region after removal of mPEG-sil was modified by linkers, APTMS and NHS-biotin, and then by the dye-labeled Streptavidin. Linker binding process used in this research has been well accepted for SA binding and has been reported in several works.[25,26] Characterization of the surface condition using FTIR[27] and XPS[28] has been demonstrated on silicon-based surface. However, the AFM scanning showed no significant change in surface roughness after subsequent modifications (see the Supporting Information, Figure S1). The removal of mPEG-sil via localized Joule heating was also characterized by AFM phase signal as shown in Figure S2 in the Supporting Information. The phase images show strong contrast along the channel of PND after localized Joule heating, while topography images exhibit very little information

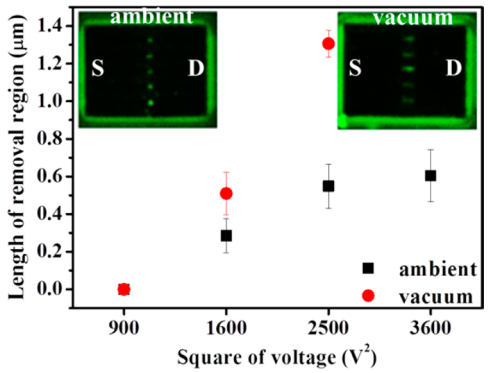

Figure 4. Plot of length of removal regions vs square of voltage. The solid black square and solid red circle represent ambient and vacuum, respectively, during localized Joule heating. The error bar was measured from the five nanobelts. Insets show the fluorescence images after dye-labeled Streptavidin binding; the left and right insets show localized Joule heating in ambient and in vacuum, respectively.

in height and surface roughness presumably due to the grain size of polysilicon (30−40 nm). Furthermore, insets in Figure 4 show the fluorescence images after binding of biotin and dye-labeled Streptavidin. Five green fluorescence regions exhibited selective binding of biotin and dye-labeled Streptavidin in the middle of the nanobelt, corresponding to the n^- regions. The lengths of removal regions after applying 40 and 50 V were 0.509 and 1.306 μm, respectively, in vacuum. However, in ambient the lengths of removal regions for applications of 40, 50, and 60 V were 0.285, 0.548, and 0.604 μm, respectively. Even though the applied bias was as high as 60 V in ambient, the length of removal regions was still shorter than that of applied 50 V in vacuum. This is due to the heat dissipation rate being slower in vacuum than in ambient,[29] such that a larger heating temperature profile (with a same temperature) was obtained in vacuum. PND was broken when the applied voltage is larger than 60 V in ambient and 50 V in vacuum; the electrical properties of PNDs were investigated that no degradation was observed before the critical voltage. The breakdown of PNDs takes place at the n^- regions and is believed resulted from the heat accumulation at the n^- region of the PND. The conductance of PND increases after localized Joule heating presumably due to the annealing of polysilicon channel (see the Supporting Information, Figure S3a). Optical image (see the Supporting Information, Figure S3b) shows the broken of PNDs at the n^- regions.

Furthermore, the vacuum environment is beneficial for removal of the mPEG-sil as a result of desorption of siloxane bonds from the surface. Under the same heating power, polymer thin film like PMMA is just in molten state and cannot be ablated (see the Supporting Information, Figure S4). Therefore, the substitution of polymer thin film by mPEG-sil and performing localized Joule heating under vacuum can maximize the removal regions effectively.

For a more comprehensive understanding of the localized Joule heating, the temperature distribution was estimated by the COMSOL simulation in 1 atm. Figure 5a shows the surface temperature distribution on the PND around n^- regions after applying 40 V pulse voltage with the temperature extracted at the end of the fifth μs. The n^- regions were 2 μm and marked in Figure 5a. The extracted profiles from the axial (A-A′) and

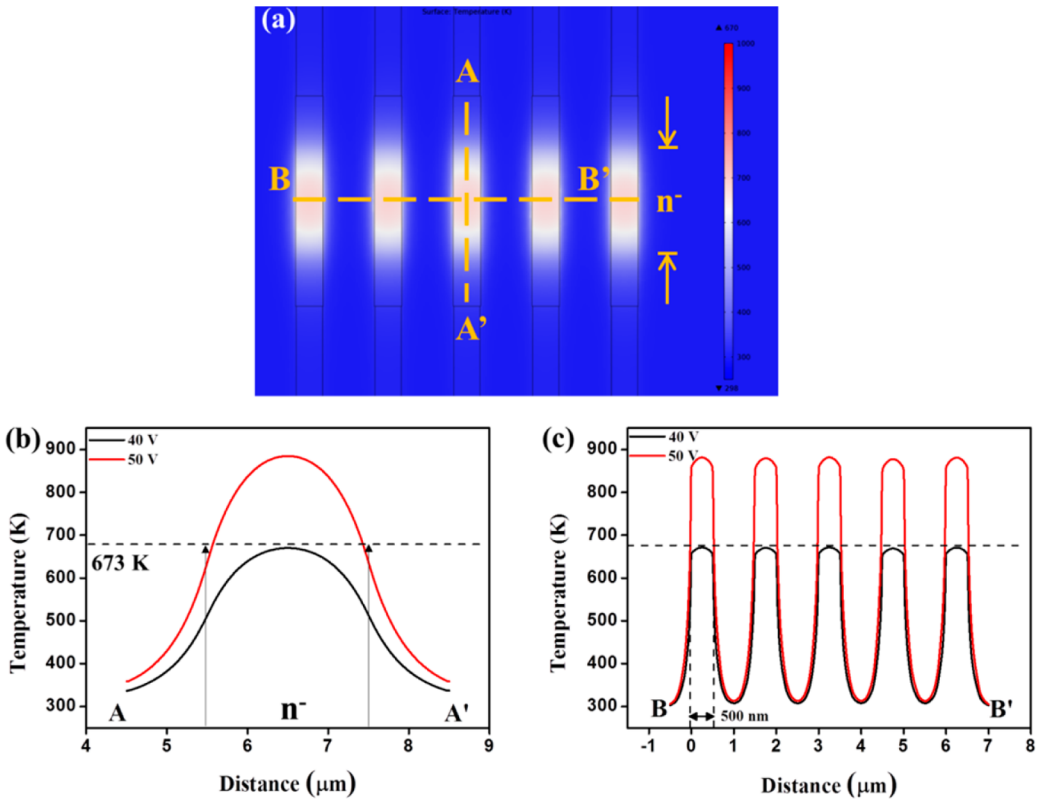

Figure 5. (a) Image of surface temperature of COMSOL simulation at 40 V pulse voltage for 5 μs. (b, c) are profiles along the axial (A−A′) and radial (B−B′) direction, respectively, and are highlighted with yellow dashed lines. The n^- region is indicated by yellow arrows. Dashed lines in b and c represent the literature value of minimum allowable temperature for silane removal. The arrows shown in b indicate the n^- region (2 μm).

dx.doi.org/10.1021/am402586q | ACS Appl. Mater. Interfaces 2013, 5, 10048−10053

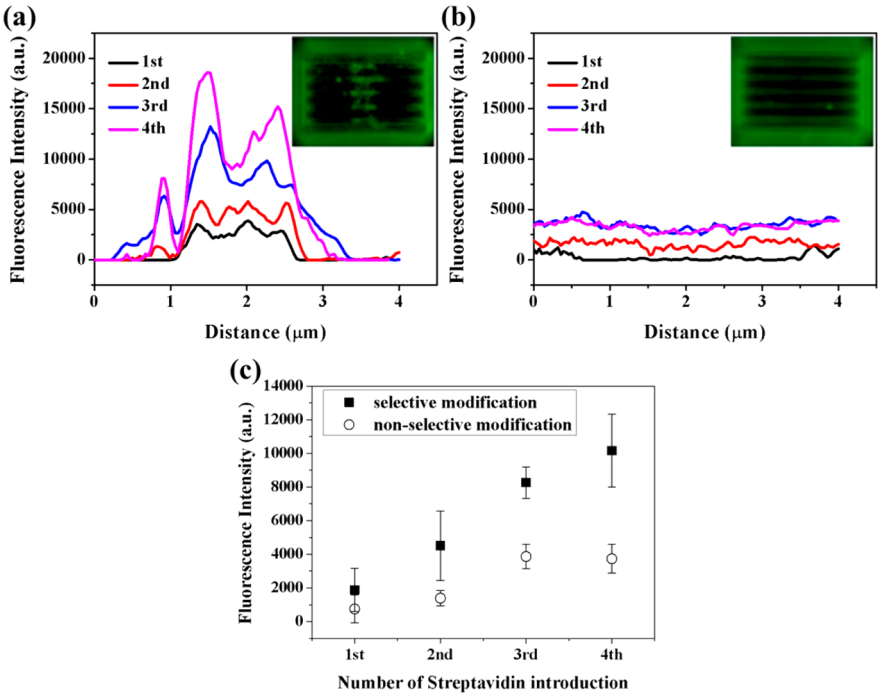

Figure 6. (a, b)Plots of fluorescence intensity vs distance along the nanobelt. Insets in a and b are the fluorescence images of the final introduction of the time-lapsed experiments. The profiles were extracted from middle one of the five nanobelts and the range was chosen along the center 4 μm. (c) Plot of the integration results from a and b, with the solid black square (■) and the open circle (○) representing the average intensities in the profiles for selective modification and nonselective modification, respectively, n = 3.

radial direction (B−B′) (dashed lines labeled in Figure 5a) are shown in Figure 5b,c. From the axial distribution profile, the peak temperatures for application of 40 and 50 V were 670 and 877 K, respectively. Because a siloxane bond (Si−O−Si) breaking energy requires a temperature over 1000 K, however, this implies that the siloxane bond can be transformed into a transition state with lower activation energy during the heating process.[30] The temperature for silane desorption was reported be at least 673 K.[31,32] The experimental data showed that the lowest applied Joule heating voltage to remove mPEG-sil was 40 V, and these simulation results showed that the peak temperature in the n^- regions is very close to 673 K. In addition, the phenomenon of heat confinement in the n^- regions was also demonstrated by COMSOL simulation. The temperature profile in the axial direction showed a Gauss distribution and the distance between two points where temperatures were higher than 673 K for 50 V was 1.862 μm, located within the n^- region.

The temperature profiles along the radial direction showed that the temperature beyond the margins of nanobelts decreases rapidly and is under 673 K for both applied voltages, as shown in Figure 5c. A temperature higher than 673 K was maintained in the nanobelts. Moreover, the temperature rate increases faster than 0.8 K/ns, which implies 5 μs heating time is sufficient to remove mPEG-sil. On the other hand, simulations for the longer n^- regions were also evaluated (see the Supporting Information, Figure S5a). Under the same pulse power, the peak temperature for PNDs with 5 and 10-μm n^- region were 455 and 343 K, respectively. To reach 673 K, the pulse voltage of 81 and 140 V are required for PNDs with 5 and 10 μm n^- region, respectively (see the Supporting Information, Figure S5b).

The experiments for reducing sensing time were examined with selective and nonselective biotin-modified PNDs in microfluidic channels, and shown in Figure 6. Dye-labeled Streptavidin with a concentration of 10 μg/mL was pumped through a 1.6-μL microfluidic channel with a volume flow rate of 100 μL/min for 30 s. After each introduction of dye-labeled Streptavidin, we removed the microfluidic channel and washed the chip rigorously with 1X PBST and then observed fluorescence intensity. A total of four successive introductions were performed. The profiles of fluorescence intensity were extracted in the middle of the 5 nanobelts along the axial direction. Results showed that the PND with selective modification exhibited an obvious increment in peak intensity after each introduction of dye-labeled Streptavidin; the peak intensity after the last introduction reached a maximum, as shown in Figure 6a. In the meantime, the intensity outside the removal regions remained at a low fluorescence level, implying good passivation of mPEG-sil. In contrast, the profiles of intensity for the nonselective modification samples exhibited only a minor increase in fluorescence intensity after the four introductions of dye-labeled Streptavidin, as shown in Figure 6b. Figure 6c shows an integrated result for time-lapsed measurement for both selective and nonselective modification devices. We observed that the intensity increases linearly with each introduction of dye-labeled Streptavidin for both cases, and the increasing intensity rate was enhanced by a magnitude of ~2×X for the selectively modified one. The experiments were repeated three times with high consistency.

The green fluorescence appeared at outer regions for both control and sensing samples is referred to background fluorescence. (see the Supporting Information, Figure S6). Additional experiments using PND and silicon nanobelt field-effect transistor (SNFET) have also been performed for real-time detection of SA at various concentrations. Fluorescence intensity shows that the LOD for selective modified PND is 1 μg/mL, and nonselective modification case is 10 μg/mL. On

the other hand, the SNFET is sensitive to changes of surface potential as a result of SA binding at the high sensitive region. The LOD is 15 pM for selective modified SNFET and 150 pM for nonselective modified device. The LOD in both cases is improved by one order (see the Supporting Information, Figure S7)

4. CONCLUSION

In this study, polysilicon nanodevices (PNDs) were successfully manufactured by a conventional CMOS technique with a designed two-level doping profile along the channel. Localized Joule heating with pulse power and selective modification onto regions of PNDs were both achieved. A well-packaged SAM (mPEG-sil) as a protection layer effectively inhibits the nonspecific binding on PNDs. Utilizing SAM mPEG-sil and performing localized Joule heating in vacuum reduces Joule heating power. Joule heating in vacuum also maximized the removal regions of mPEG-sil around the n^- region, which can be beneficial for further applications in electrical detection. Finally, time-lapsed observation fluorescence intensity in the microfluidic channel verified the increasing rate of intensity of a magnitude of ~2× in the selectively modified PND.

■ ASSOCIATED CONTENT

Supporting Information

Figure S1, AFM topography images of surface condition on blank oxide chip, APTMS modification, and NHS-biotin modification; Figure S2, topology and phase image of PND before and after mPEG-sil removal via localized Joule heating; Figure S3, electrical characteristics of PND before and after localized Joule heating; Figure S4, AFM topography image of PND after localized Joule heating of PMMA passivation; Figure S5, COMSOL simulations of temperature distribution of PND with various n^- region; Figure S6, background fluorescence in outer region of PND; Figure S7, LOD investigation using optical and electrical detection. This material is available free of charge via the Internet at http://pubs.acs.org.

■ AUTHOR INFORMATION

Corresponding Author

*E-mail: jtsheu@faculty.nctu.edu.tw.

Notes

The authors declare no competing financial interest.

■ ACKNOWLEDGMENTS

The authors thank MOE-ATU program and National Science Council (NSC 101-2120-M-009-011-CC1) in Taiwan for financial support.

■ REFERENCES

(1) Cui, Y.; Wei, Q. Q.; Park, H. K.; Lieber, C. M. *Science* **2001**, *293*, 1289−1292.
(2) Hahm, J.; Lieber, C. M. *Nano Lett.* **2004**, *4*, 51−54.
(3) Patolsky, F.; Zheng, G. F.; Hayden, O.; Lakadamyali, M.; Zhuang, X. W.; Lieber, C. M. *Proc. Natl. Acad. Sci. U.S.A.* **2004**, *101*, 14017−14022.
(4) Patolsky, F.; Zheng, G. F.; Lieber, C. M. *Nanomedicine* **2006**, *1*, 51−65.
(5) Patolsky, F.; Lieber, C. M. *Mater. Today* **2005**, *8*, 20−28.
(6) Patolsky, F.; Zheng, G. F.; Lieber, C. M. *Anal. Chem.* **2006**, *78*, 4260−4269.
(7) Stern, E.; Klemic, J. F.; Routenberg, D. A.; Wyrembak, P. N.; Turner-Evans, D. B.; Hamilton, A. D.; LaVan, D. A.; Fahmy, T. M.; Reed, M. A. *Nature* **2007**, *445*, 519−522.
(8) Sheu, J. -T.; Chen, C. C.; Chang, K. S.; Li, Y. K. *Biosens. Bioelectron.* **2008**, *23*, 1883−1886.
(9) Kim, D. R.; Zheng, X. L. *Nano Lett.* **2008**, *8*, 3233−3237.
(10) Leyden, M. R.; Messinger, R. J.; Schuman, C.; Sharf, T.; Remcho, V. T.; Squires, T. M.; Minot, E. D. *Lab Chip* **2012**, *12*, 954−959.
(11) Masood, M. N.; Chen, S.; Carlen, E. T.; van den Berg, A. *ACS Appl. Mater. Interfaces.* **2010**, *2*, 3422−3428.
(12) Li, B. R.; Chen, C. W.; Yang, W. L.; Lin, T. Y.; Pan, C. Y.; Chen, Y. T. *Biosens. Bioelectron.* **2013**, *45*, 252−259.
(13) Herzer, N.; Hoeppener, S.; Schubert, U. S. *Chem. Commun.* **2010**, *46*, 5634−5652.
(14) Wang, D. W.; Thomas, S. G.; Wang, K. L.; Xia, Y. N.; Whitesides, G. M. *Appl. Phys. Lett.* **1997**, *70*, 1593−1595.
(15) George, A.; Knez, M.; Hlawacek, G.; Hagedoorn, D.; Verputten, H. H. J.; van Gastel, R.; ten Elshof, J. E. *Langmuir* **2012**, *28*, 3045−3052.
(16) Rosso, M.; Giesbers, M.; Schroën, K.; Zuilhof, H. *Langmuir* **2010**, *26*, 866−872.
(17) Piner, R. D.; Zhu, J.; Xu, F.; Hong, S. H.; Mirkin, C. A. *Science* **1999**, *283*, 661−663.
(18) Iversen, L.; Younes-Metzler, O.; Martinez, K. L.; Stamou, D. *Langmuir* **2009**, *25*, 12819−12824.
(19) Park, I.; Li, Z. Y.; Pisano, A. P.; Williams, R. S. *Nano Lett.* **2007**, *7*, 3106−3111.
(20) Chen, C. C.; Lin, Y. S.; Sang, C. H.; Sheu, J. -T. *Nano Lett.* **2011**, *11*, 4736−4741.
(21) Zhang, M.; Desai, T.; Ferrari, M. *Biomaterials* **1998**, *19*, 953−960.
(22) Sharma, S.; Johnson, R. W.; Desai, T. A. *Appl. Surf. Sci.* **2003**, *206*, 218−229.
(23) Choi, I.; Kang, S. K.; Lee, J.; Kim, Y.; Yi, J. *Biomaterials* **2006**, *27*, 4655−4660.
(24) Lan, S.; Veiseh, M.; Zhang, M. *Biosens. Bioelectron.* **2005**, *20*, 1697−1708.
(25) Stern, E.; Wagner, R.; Sigworth, F. J.; Breaker, R.; Fahmy, T. M.; Reed, M. A. *Nano Lett.* **2007**, *7*, 3405−3409.
(26) Duan, X. X.; Li, Y.; Rajan, N. K.; Routenberg, D. A.; Modis, Y.; Reed, M. A. *Nat. Nanotechnol.* **2012**, *7*, 401−407.
(27) Lapin, N. A.; Chabal, Y. J. *J. Phys. Chem. B* **2009**, *113*, 8776−8783.
(28) Williams, E. H.; Davydov, A. V.; Motayed, A.; Sundaresan, S. G.; Bocchini, P.; Richter, L. J.; Stan, G.; Steffens, K.; Zangmeister, R.; Schreifels, J. A.; Rao, M. V. *Appl. Surf. Sci.* **2012**, *258*, 6056−6063.
(29) Santini, C. A.; Vereecken, P. M.; Volodin, A.; Groeseneken, G.; De Gendt, S.; Haesendonck, C. V. *Nanotechnology* **2011**, *22*, 395202−395210.
(30) Camino, G.; Lomakin, S. M.; Lazzari, M. *Polymer* **2001**, *42*, 2395−2402.
(31) Yildirim, A.; Ozgur, E.; Bayindir, M. *J. Mater. Chem. B* **2013**, *1*, 1909−1920.
(32) Zhuang, Y. X.; Hansen, O.; Knieling, T.; Wang, C.; Rombach, P.; Lang, W.; Benecke, W.; Kehlenbeck, M.; Koblitz, J. *J. Micromech. Microeng.* **2006**, *16*, 2259−2264.